Optical characterization of wide band gap amorphous semiconductors (a-Si:C:H): Effect of hydrogen dilution

Cite as: Journal of Applied Physics **89**, 1130 (2001); https://doi.org/10.1063/1.1332421
Submitted: 10 August 2000 • Accepted: 18 October 2000 • Published Online: 29 December 2000

Minseo Park, C. W. Teng, V. Sakhrani, et al.

Optical characterization of wide band gap amorphous semiconductors (*a*-Si:C:H): Effect of hydrogen dilution

Minseo Park[a)]
Department of Materials Science and Engineering, North Carolina State University, Raleigh, North Carolina 27695

C. W. Teng
Department of Electrical and Computer Engineering, North Carolina State University, Raleigh, North Carolina 27695

V. Sakhrani and M. B. McLaurin
Department of Materials Science and Engineering, North Carolina State University, Raleigh, North Carolina 27695

R. M. Kolbas
Department of Electrical and Computer Engineering, North Carolina State University, Raleigh, North Carolina 27695

R. C. Sanwald
Department of Materials Science and Engineering, North Carolina State University, Raleigh, North Carolina 27695

R. J. Nemanich
Department of Physics, North Carolina State University, Raleigh, North Carolina 27695

J. J. Hren and J. J. Cuomo
Department of Materials Science and Engineering, , North Carolina State University, Raleigh, North Carolina 27695

(Received 10 August 2000; accepted for publication 18 October 2000)

The effect of hydrogen dilution on the optical properties of a wide band gap amorphous semiconductor (*a*-Si:C:H) was investigated. The samples were prepared by glow discharge decomposition of tetramethylsilane and were characterized primarily by optical techniques: spectroscopic ellipsometry, Raman scattering, infrared absorption, spectrophotometry, and UV photoluminescence. The deposition rate decreased with hydrogen dilution, while the silicon to carbon ratio remained constant with the addition of hydrogen. The optical band gap of this material increased as the hydrogen flow rate increased. Infrared absorption studies show that the concentration of hydrogen which is bonded to carbon decreases systematically upon hydrogen dilution. Hydrogen dilution appears to reduce the size and concentration of sp^2 bonded carbon clusters, possibly caused by the etching of sp^2 clusters by atomic hydrogen. The result was also supported by the shift of the Raman *G* peak position to a lower wave number region. Room temperature photoluminescence in the visible spectrum was observed with UV excitation. [DOI: 10.1063/1.1332421]

I. INTRODUCTION

Great interest has been focussed on wide band gap amorphous silicon–carbon (*a*-Si:C:H) because of the wide range of potential applications in photonics. This material can be used in the fabrication of devices such as flat panel displays and solar cells.[1,2] Large area deposition on low cost substrates can be easily achieved by amorphous semiconductor technology. At present, the major application of *a*-Si:C:H is to increase the efficiency of the window layer in photovoltaic cells. In this structure, the band gap widening of amorphous silicon (*a*-Si:H) upon carbon incorporation was utilized.[3] Luminescence in the visible spectrum has been observed by many researchers.[4,5] Light emitting devices for electroluminescence flat panel displays have been fabricated and their room temperature operation demonstrated.[6] Rüter *et al.* fabricated luminescent waveguiding layer structures with *a*-Si:C:H, and it was proposed that this material could be used as a fast, sensitive, and selective UV detector.[7]

In the present study, we used tetramethylsilane (TMS) as a precursor since carbon-rich *a*-Si:C:H films can easily be produced from this source. A carbon-rich composition of *a*-Si:C:H was chosen in order to produce a material with a band gap close to that of crystalline 6H-SiC ($E_g = 3.1$ eV). The structure of carbon-rich *a*-Si:C:H can be considered as silicon containing diamond-like carbon or hydrogenated amorphous carbon (*a*-C:H). The basic building blocks of all carbon allotropes are *sp*, sp^2, and sp^3 hybrid orbital. In diamond, carbon atoms form strong hybrid sp^3 orbitals. Each

a)Author to whom correspondence should be addressed; electronic mail: mpark2@eos.ncsu.edu

TABLE I. Deposition parameters for the growth of *a*-Si:C:H.

Gas flow rate	
TMS	1.5 sccm
Ar (carrier for TMS)	45 sccm
H_2	0–300 sccm
Pressure	50 mTorr
Substrate bias	−300 V
rf power	200 W
Deposition time	30 min

carbon atom is tetrahedrally coordinated with bonding angles of 109° 28′. In the graphite structure, the carbon bonds are composed of σ (sp^2 hybrid) and π (p_z). The strong covalent σ bonds form angles of 120° to each other, while the delocalized out-of-plane π (p_z) orbitals bond planes together with weak van der Waals force. Amorphous carbon [*a*-:C:(H)] is composed of both graphite-like sp^2 and diamond-like sp^3 sites. It has been suggested that the sp^2 sites have a tendency to form clusters in an amorphous sp^3 bonded carbon matrix in order to maximize the π bonding energy.[8,9]

The effect of hydrogen dilution on the structural and optical properties of *a*-Si:C:H has been investigated.[10,11] However, the influence of hydrogen in this material has not been understood completely. In this investigation, we have explored the role and effect of hydrogen dilution on the optical and structural properties of carbon-rich amorphous silicon carbon (*a*-Si:C:H) produced by glow discharge decomposition of TMS. A variety of optical diagnostic techniques were utilized for sample characterization, and the results from these methods were compared. Optical characterization is a powerful nondestructive evaluation technique for thin film analysis.

II. EXPERIMENTAL PROCEDURE

A. Sample preparation

The hydrogenated amorphous silicon–carbon (*a*-Si:C:H) thin films were deposited onto Si(100) and sapphire using a capacity coupled 13.56 MHz rf plasma enhanced chemical vapor deposition. The deposition was performed with TMS while varying the concentration of hydrogen. The rf power was 200 W, the substrate bias was −300 V, and the chamber pressure was 50 mTorr. The details of the processing conditions are summarized in Table I.

B. Characterization

The films were analyzed by profilometry, Auger electron spectroscopy, spectroscopic ellipsometry, micro-Raman scattering, infrared absorption, optical transmission, and photoluminescence spectroscopy.

Auger electron spectroscopy was performed using 10 keV primary electrons, at a probe current of 1.61 microamps, in a JEOL JAMP-30 scanning Auger microprobe. The angle of incidence of the primary electron beam relative to the surface normal was 30°. The energy resolution of the cylindrical mirror analyzer was ~0.7%. Sputter etching was performed by rastering a 3 keV, ~400 nA Ar ion beam for ~25 s. The spectra were acquired in a derivative mode at a base pressure of 2.25×10^{-9} Torr.

A commercial Woollam VASE 700 rotating-analyzer ellipsometer was used for the spectroscopic ellipsometry. Broadband light produced by a xenon arc discharge lamp was focused into the monochromator, using a Czerny–Turner scanning monochromator with the standard 1200 line/mm ruled gratings. After collimation and polarization, the beam was incident on the sample, and the angle between the incident beam and the sample surface normal was 75°. The analyzer contains a Glan–Taylor polarizer, and the signal was processed and analyzed using WVASE32™ software. The ellipsometer was calibrated with ~255 Å SiO_2/Si wafer.

Micro-Raman spectroscopy was carried out at room temperature using backscattering geometry with the 514.5 nm line of an Ar ion laser. A ISA U-1000 scanning double monochromator was used to collect the Stokes spectra. Since the diameter of the focused laser beam was ~5 μm, it was possible to analyze local structures using the micro-Raman techniques. A Dilor LabRam micro-Raman spectrometer was also used for Raman scattering experiments. scattering experiments. The 632.8 nm line of a He–Ne laser was illuminated onto the sample with a microscope, and the spectra were collected with a multichannel charge coupled device detector.

The Fourier transform infrared (FTIR) spectroscopy was performed using a BOMEM FTIR spectrometer. Optical transmission measurements were taken on a dual beam Cary 5E ultraviolet-visible-near-infrared (UV–VIS–NIR) spectrophotometer at room temperature. Photoluminescence spectra were excited with a continuous wave argon-ion laser (270–305 nm) and the emission was focused upon a 0.64 m spectrometer equipped with an S-20 photocathode.

III. RESULTS AND DISCUSSION

A. Deposition rate and composition

Figure 1(a) shows the film thickness as a function of hydrogen flow rate, which was measured by profilometry. The deposition rate of the hydrogenated amorphous silicon carbon (*a*-Si:C:H) film decreased as the concentration of hydrogen in the reactor increased.

The composition of the films were determined by Auger electron spectroscopy (AES). The Si/C ratio determined using the *KLL* peaks for Si and C was 1:2, which did not change with hydrogen dilution [Fig. 1(b)]. The oxygen signal was observed from the AES surface scan. However, subsurface scans after Ar ion etching did not display any oxygen signature, and the bulk film appears free of oxygen.

B. Spectroscopic ellipsometry

Spectroscopic ellipsometry was performed on carbon-rich *a*-Si:C:H films in order to extract information about the variation in dielectric constant, refractive index, and the electron energy loss function as a function of hydrogen flow rate. The intensity of the detected light with a rotating analyzer ellipsometer is expressed by[12,13]

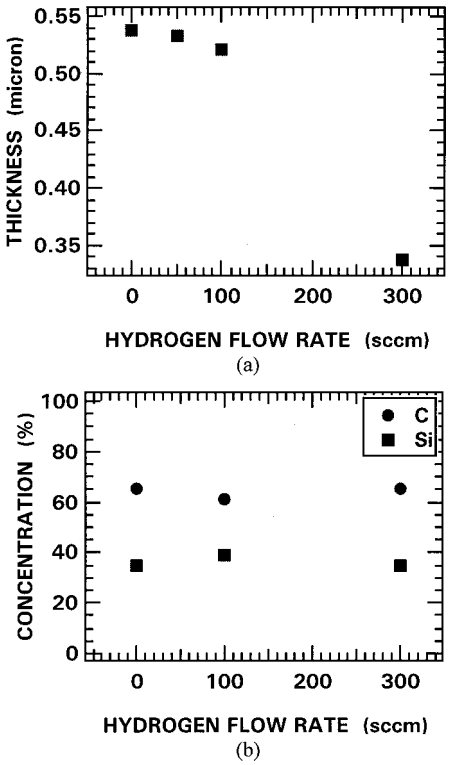

FIG. 1. (a) Thickness of the film as a function of hydrogen flow rate. (b) Concentration of Si and C in *a*-Si:C:H as a function of hydrogen flow rate.

$$I(\theta) = I_0[1 + \alpha \cos(2\theta) + \beta \sin(2\theta)], \tag{1}$$

where I_0 is the average intensity, α and β are the normalized Fourier coefficients, and θ is the instantaneous analyzer azimuth angle.

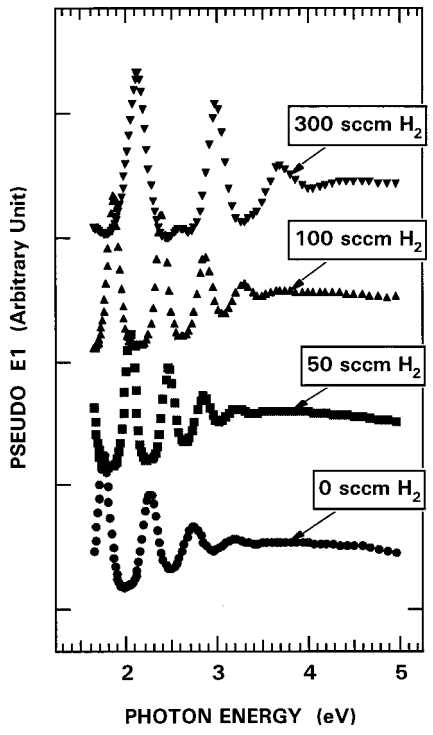

FIG. 2. Pseudodielectric function as a function of hydrogen flow rate.

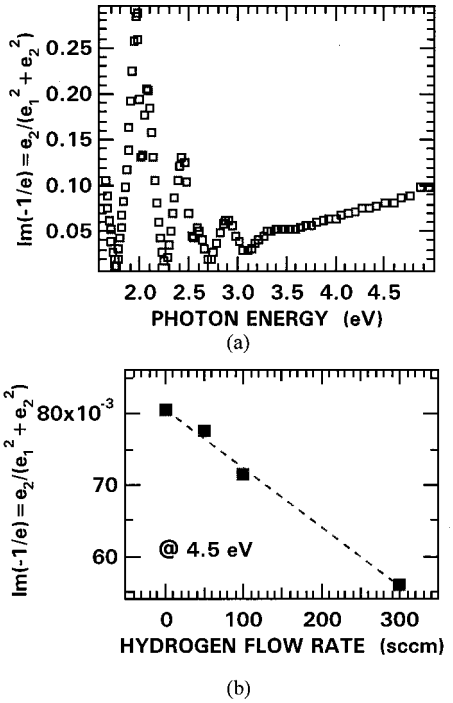

FIG. 3. (a) EEL function and (b) change in EEL function at 4.5 eV photon energy as a function of hydrogen flow rate.

Figure 2 shows the dielectric response from *a*-Si:C:H/Si as a function of the hydrogen flow rate. As seen in the figure, the point where the interference pattern stops is shifted to a higher energy as the H_2 concentration is increased. This implies that the optical band gap of this material widens upon hydrogen dilution. The band gap widening was also evident in an optical absorption experiment (see a later section for discussion).

The electron energy loss (EEL) spectrum due to inelastic scattering can be analyzed by the electron energy loss function, which is defined by

$$\mathrm{Im}-\left[\frac{1}{\tilde{\epsilon}}\right] = \frac{\epsilon_2}{\epsilon_1^2 + \epsilon_2^2}. \tag{2}$$

In an *a*-C EEL spectrum, plasmon or collective excitation of the π and $\sigma+\pi$ electron produces energy loss peaks at $\sim$7 and 31 eV, respectively.[14] However, we did not observe these features in our EEL spectrum [Fig. 3(a)] due to the low photon energy used ($<$5 eV). Nevertheless, it can be clearly seen that the EEL function increases with increasing photon energy, which is indicative of the increasing contributions from the π electron as the photon energy approaches the π electron plasmon peak at $\sim$7 eV. Figure 3(b) shows the EEL function measured at 4.5 eV as a function of hydrogen flow rate. The decrease in the absolute value of the EEL function may mean that the influence from the π electron diminishes with hydrogen dilution. This interpretation is strongly supported by Raman spectroscopy, which will be discussed later. Another point to be addressed is that shift in the π plasmon peak can also produce a reduction in the absolute value of the EEL function in our spectrum. It was

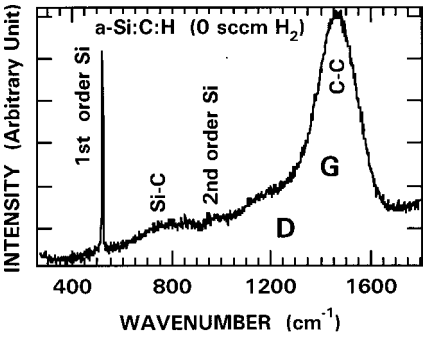

FIG. 4. Raman spectrum of *a*-Si:C:H.

found that the π plasmon peak shifts toward a lower energy when more sp^2 bonded carbon clusters are formed in increasing nitrogen content in a-CH:N_x.[15]

C. Raman scattering

1. Normal Raman scattering

Figure 4 shows a first-order Stokes Raman spectrum from amorphous silicon-carbon produced at various hydrogen flow rates. The firs order Raman spectrum reflects the density of vibrational states in this material. The broad feature near 1500 cm^{-1} is attributed to the first order Raman scattering due to the C–C bond. It is known that the position of both the *D* and *G* peak of amorphous carbon shifts to a lower wave number as Si is incorporated into the film.[16] It has been proposed that the decrease of the Raman frequency upon Si addition occurs because the C–C bond is stronger than the Si–C bond and C atoms are lighter than Si atoms.

Only a weak Raman peak due to the Si–C bond was observed, since the bond polarizability of the C–C bond is approximately 40 times higher than the Si–C bond.[17] The peaks at 520 cm^{-1} and at about 970 cm^{-1} were produced by first- and second-order Raman scattering from the Si substrate, respectively. The structure of the carbon-rich amorphous silicon–carbon is close to that of amorphous carbon, so the Raman spectrum can be analyzed relative to that of amorphous carbon. The typical Raman spectrum of amorphous carbon consists of two broad bands; a *G* band (*G* for graphite) at about 1580 cm^{-1} and *D* band (*D* for disordered) at approximately 1350 cm^{-1}. The crystal structure of graphite belongs to the D_{6h}^4 space group, and has 12 vibrational modes at the Brillouin zone center ($k=0$).[18] The irreducible representation for zone center optic modes can be expressed as[19]

$$\Gamma = A_{2u} + 2B_{2g} + E_{1u} + 2E_{2g}. \tag{3}$$

The E_{2g} modes are Raman active and are measured as two in-plane vibrational modes; a low frequency E_{2g1} mode (42 cm^{-1}) and a high frequency E_{2g2} mode (1581 cm^{-1}).[19] The E_{2g2} mode is frequently referred to as the *G* band in amorphous carbon literature. The *D* band is related to the disorder-induced A_{1g} mode at the *K* point in the Brillouin zone of graphite.[20] When long-range translational symmetry is lost due to bond-angle disorder upon amorphization, the selection rule is destroyed. Thus, optical phonons with any *k* vector in the Brillouin zone can contribute to Raman scattering.

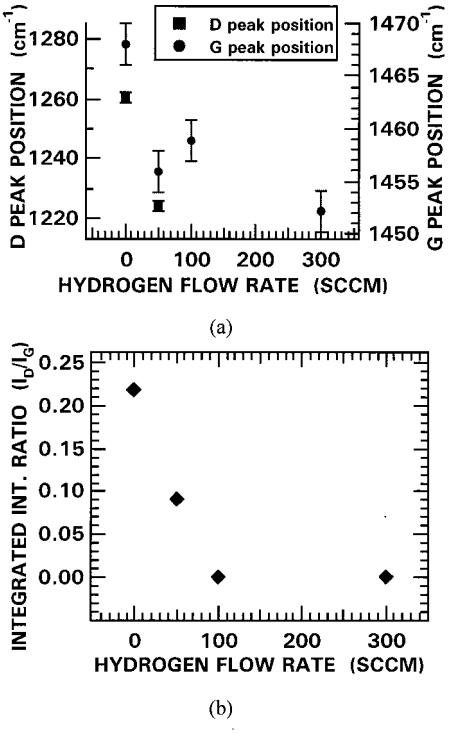

FIG. 5. (a) Shift in *G* and *D* peak position and (b) change in I_D/I_G as a function of hydrogen flow rate.

The position and full width at half maximum (FWHM) of the peaks were obtained by fitting the peak with two Gaussian functions and a linear background. The curve fitting was performed iteratively with the Levenberg–Marquardt algorithm until the chi squared

$$\chi^2 = \Sigma \left(\frac{I^{\text{cal}} - I^{\text{exp}}}{\sigma_I} \right)^2 \tag{4}$$

is minimized, where σ_I is the standard deviation.

In a typical Raman spectrum for amorphous carbon, the position of the *G* band shifts significantly if the sp^2/sp^3 carbon ratio of the film varies.[21,22] The shift in frequency of the Raman spectrum can be produced by changes in the force constant due to a change in sp^2/sp^3 carbon ratio. As is seen from Fig. 5(a), the position of the *G* peak shifts to the lower wave number region as the gas flow rate of hydrogen increases. This shift implies that a fraction of sp^2 bonded carbon atoms are reduced upon hydrogen dilution.

Figure 5(b) shows a change in the integrated intensity ratio of the *D* peak to the *G* peak (I_D/I_G). The ratio I_D/I_G decreases as H flow is increased, and the contribution from the *D* peak completely disappeared at a hydrogen flow rate of 100 sccm. Tuinstra and Koenig found that the I_D/I_G ratio increases as the in-plane crystallite size L_a decreases.[23] However, as will be explained in a later section of this article, this is contrary to our empirical observation that the band gap of this material increases upon hydrogen dilution. The increase in band gap is likely produced by a reduction in cluster size. It was also proposed by Bhargava *et al.* that I_D/I_G can in-

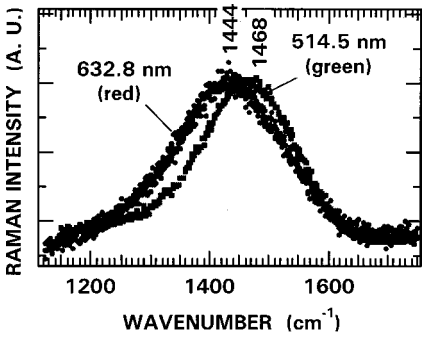

FIG. 6. Excitation frequency dependant Raman scattering of *a*-Si:C:H.

crease upon reduction in disorder, and this was supported by the observed increase in the number of regions with six membered rings observed by Scanning tunneling microscopy.[24]

It was also suggested that I_D/I_G increases as the size of the graphitic crystallites increases for crystal sizes smaller than ~2.5 nm.[25,26] The generally accepted view on the interpretation of the change in I_D/I_G is that this ratio increases as the crystallite size decreases, and begins to decrease when the size of the clusters becomes smaller than 1.2–2.5 nm.[27] For crystallites smaller than 1.2–2.5 nm, the smaller I_D/I_G, the smaller the cluster size, which in turn means a lower fraction of sp^2 carbon bonds in the film. Therefore, it can be concluded that a lower fraction of sp^2 bonded carbon was produced by hydrogen dilution.

Based on the trend in the Raman spectra, it appears that hydrogen dilution promotes an increase in the bond-angle disorder (i.e., reduction in short-range order) and a reduction in the size and number of sp^2 clusters in *a*-Si:C:H.

2. Excitation frequency-dependent Raman scattering

Figure 6 shows the excitation energy dependent Raman spectra of *a*-Si:C:H. As is seen from the figure, the position of the Raman *G* peak shifted roughly 24 cm^{-1} to a lower frequency when the wavelength of the excitation laser was 632.8 nm. It is believed that this frequency shift was caused by resonant Raman scattering from sp^2 bonded clusters of various sizes. If the energy of the exciting laser is close to that of the electronic transition, resonance Raman scattering occurs, resulting in significant enhancement in the intensity. In the case of *a*-C(:H), the electronic π to π^* transition occurs in the range of 3.5–6.5 eV.[14] A resonant Raman scattering effect from *a*-C has been observed by Wagner *et al.*[28] It was shown that the *a*-C Raman peak shifted to a higher frequency with increasing excitation photon energy. In our spectra, the same trend was observed, implying that carbon-rich *a*-Si:C:H can be explained the same way as that for *a*-C(:H). It appears that our film is composed of a broad distribution of different sized carbon clusters, and the different cluster sizes can be probed by changing excitation energy. Further research on the excitation frequency-dependent Raman scattering effect in this material is in progress, and the result will be reported elsewhere.

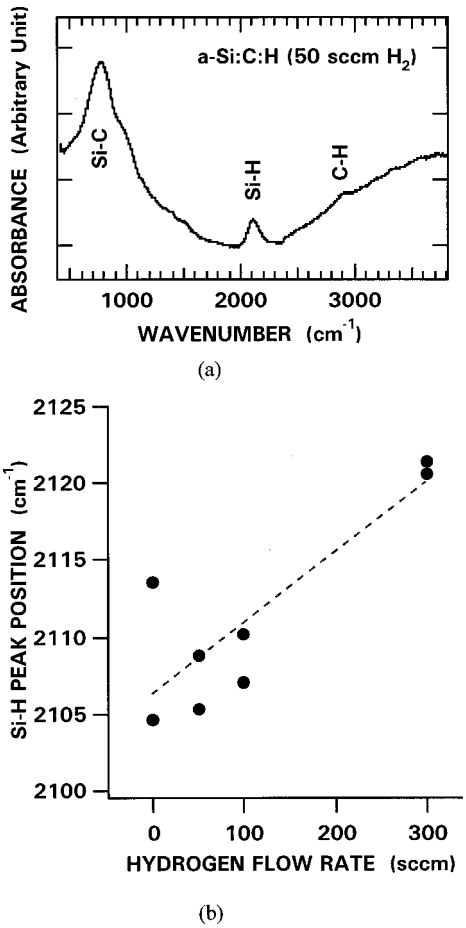

FIG. 7. (a) FTIR spectrum of *a*-Si:C:H. (b) Shift in Si–H peak position as a function of hydrogen flow rate.

D. Infrared absorption

Figure 7(a) shows the infrared absorption spectrum of carbon-rich *a*-Si:C:H. A wealth of bonding information was obtained from the spectra. The peak at 670 cm^{-1} could be associated with a Si–C stretching mode or SiH_n wagging.[29,30] The mode at 780 cm^{-1} is due to Si–CH_3 rocking/wagging or Si–C stretching.[30,31] The absorption band at 845 and 890 cm^{-1} is attributed to $(SiH_2)_n$ bending.[29] The 1000 cm^{-1} peak is due to CH_n wagging.[29] The peak at 2000 and 2090 cm^{-1} are associated with a Si–H and Si–H_2 stretching mode.[32] The 2000 cm^{-1} mode shifts to a higher wave number when C is bonded to Si.[31] This is produced by the increase in electronegativity due to C substitution, which shortens the Si–H distance and increases the vibrational frequency of Si–H bonds.[33] The broad peak at 2900 cm^{-1} was produced by C–H vibrations.[34,35] The IR absorption band assignment is summarized in Table II.

The broad Si–H_n absorption peak was fitted with two Gaussians and a linear background. From this curve fitting, it was found that the 2000 cm^{-1} peak position tends to shift to a higher wave number upon hydrogen dilution [Fig. 7(b)]. As was discussed earlier, the upward shift of this peak may be caused by the increasing numbers of C to Si bonds.

TABLE II. Mode assignment of infrared absorption band appears in Ir spectrum of *a*-Si:C:H.

Ir absorption band (cm^{-1})	Modes	References
670	SiC stretching	29
	SiH_n wagging	30
780	$SiCH_3$ rocking/wagging	31
	SiC stretching	30
845,890	$(SiH_2)_n$ bending	29
1000	CH_n wagging	29
2000	SiH stretching	32
2090	SiH_2 stretching	32
2800–3100	CH vibration	34,35

The concentration of hydrogen which is bonded to C and Si can be deduced from the IR spectrum using the following expression:

$$N_{H_{C-H}} = A_{C-H} \int \frac{\alpha(\omega)}{\omega} d\omega \tag{5a}$$

and

$$N_{H_{Si-H}} = A_{Si-H} \int \frac{\alpha(\omega)}{\omega} d\omega, \tag{5b}$$

where $N_{H_{C-H}}$ and $N_{H_{Si-H}}$ are the concentration of hydrogen determined by C–H and Si–H stretching modes, respectively, α is the absorption coefficient, and $A_{C-H} = 1.35 \times 10^{21}$ cm^{-2},[36] $A_{Si-H} = 1.4 \times 10^{20}$ cm^{-2}.[37] The concentration of H bonded to C decreases slightly upon hydrogen dilution (Fig. 8), which appears to be caused by the etching of sp^2 bonded carbon clusters by atomic hydrogen. It should be noted that this does not represent the total hydrogen concentration in the film. One of the main problems of the infrared absorption study is that only those carbon atoms which are bonded to hydrogen can be detected. It was previously reported in a nuclear magnetic resonance study, that hydrogen atoms are preferably bonded to sp^2 hybridized carbon and up to 65% of the carbon is not bonded to hydrogen.[38]

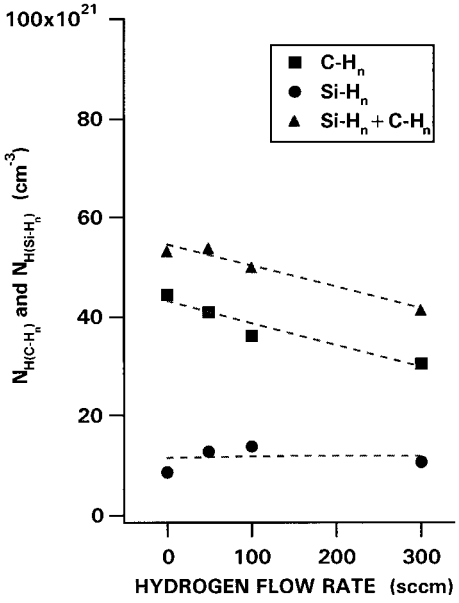

FIG. 8. Concentration of H bonded to Si and C.

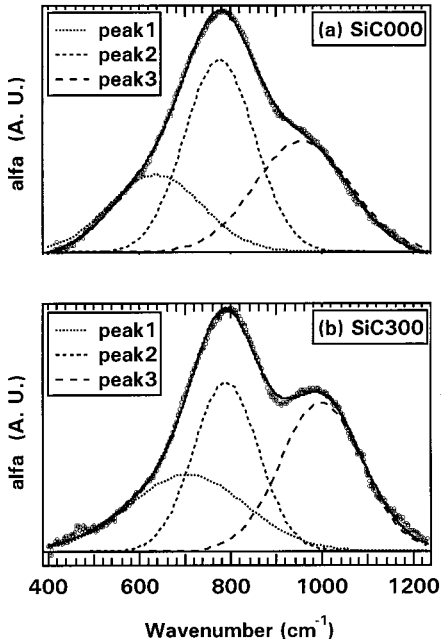

FIG. 9. Curve fitting of the Ir absorption peaks at 400–1200 cm^{-1} with three Gaussians and a linear background.

The IR absorption peaks at 400–1200 cm^{-1} were fitted with three Gaussian peaks (670, 790, and 1000 cm^{-1}) and a linear background, as shown in Fig. 9. It appears that all three peaks shift to a higher frequency upon H addition (Fig. 10). However, it is not clear at present why this shift occurs.

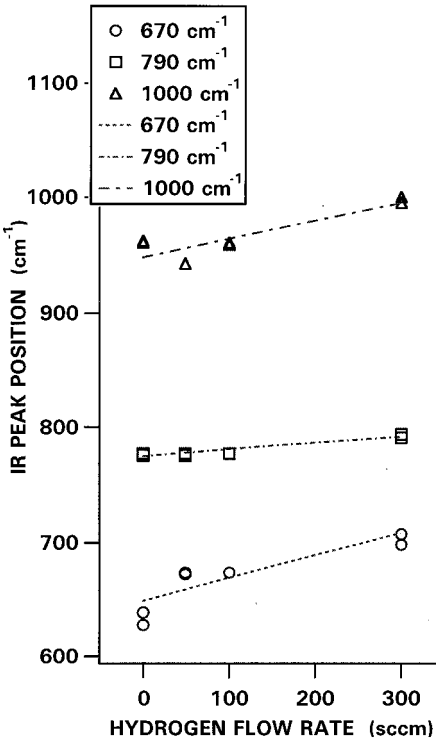

FIG. 10. Shift in 670, 790, and 1000 cm^{-1} IR peak position as a function of hydrogen flow rate.

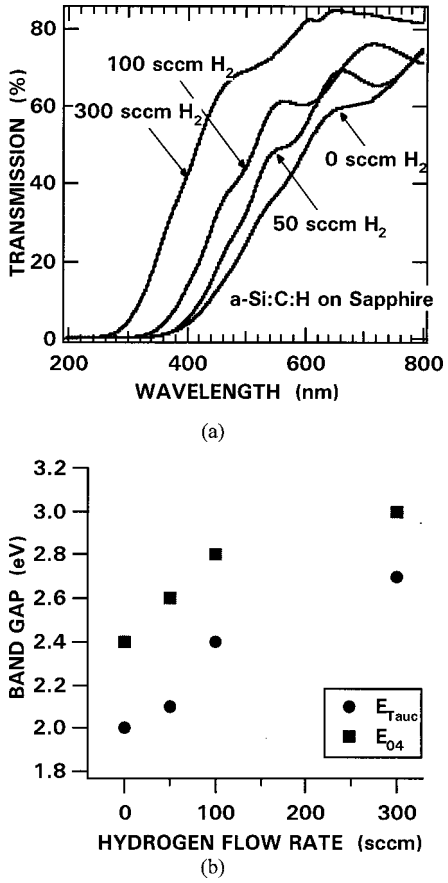

FIG. 11. (a) Optical transmission spectra of *a*-Si:C:H. (b) Change in optical band gap as a function of hydrogen flow rate.

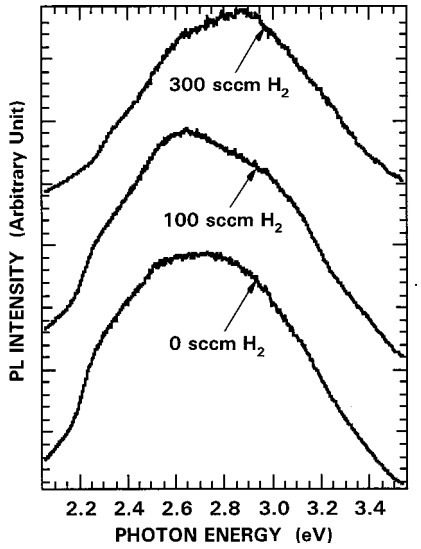

FIG. 12. Room temperature UV photoluminescence spectra of *a*-Si:C:H.

E. Optical absorption

The optical transmission spectra for *a*-Si:C:H films deposited at different H flow rates were obtained by transmission measurements and are shown in Fig. 11(a). The ''Tauc'' optical band gap E_g^{Tauc} can be obtained by fitting the absorption data to the following expression:[39]

$$\alpha(\hbar\omega)\hbar\omega = C^2(\hbar\omega - E_g^{\mathrm{Tauc}})^2, \tag{6}$$

where α is the absorption coefficient, $\hbar$ is Planck's constant, ω is the frequency of the radiation, and C a constant, which is the slope for the plot of $[\alpha(\hbar\omega)\hbar\omega]^{1/2}$ $(\mathrm{cm}^{-1/2}\,\mathrm{eV}^{1/2})$ vs $\hbar\omega$ (eV). Figure 11(b) shows the Tauc optical band gap E_{Tauc} and E_{04} gap of amorphous silicon-carbon as a function of hydrogen flow rate. The optical band gap increases monotonically as the hydrogen flow rate increases. The optical band gaps determined by the Tauc method were lower than the photoluminescence (PL) peaking energy of 2.6–2.9 eV. These results could be explained by the fact that the assumption for the premise of the Tauc method of a free electron like density of states is not valid.[40] However, the Tauc gap does vary systematically as the H flow rate increases. The increase in optical band gap is produced by a reduction in relative concentration of sp^2 bonded carbon. Another way of determining the optical band gap is using the E_{04} gap, which is defined as the energy at which the absorption coefficient is 10^4 cm^{-1}. This is an arbitrary way of defining the optical band gap, and can only be used for comparing the optical gaps of identical samples produced by different processing conditions. The E_{04} gap also increases upon H dilution. Even though none of the earlier methods provide an absolute band gap value, they exhibit the same trend. Within the range of hydrogen dilution used in this experiment, the maximum band gap shift was estimated to be ~0.6 eV.

F. UV photoluminescence

The room temperature PL spectra from samples deposited at various hydrogen flow rates are shown in Fig. 12. The excitation power density is approximately 20 $\mathrm{W/cm}^2$ and no UV radiation damage was observed on the samples. All samples emit very broad white luminescence peaked between 2.6 and 2.9 eV. The FWHM of the PL peaks are approximately 1 eV. The low temperature PL spectra measured at 77 K showed similar characteristics (not shown here). The spectral positions of the PL peaks do not exhibit any systematic shifts with increasing optical band gaps of the samples. This is consistent with the report by Demichelis *et al.* that the PL peak positions are not correlated with the optical band gaps.[41]

Hydrogenated amorphous carbon (*a*-C:H) exhibits a higher photoluminescence efficiency than amorphous silicon (*a*-Si:H) at room temperature. This result may be due to the strong Coulomb interactions which exist between the excited electron-hole pairs, since the dielectric constant of *a*-C:(H) is smaller than *a*-Si:H.[42,43] Due to this strong Coulomb interaction, the separation distance between electrons and holes is small and the charge carriers thermalize rapidly, promoting radiative recombination over nonradiative recombination.[43] According to Robertson's ''cluster'' model, the optical band gap of *a*-C:(H) is primarily controlled by the size of the sp^2 bonded clusters. The larger the cluster, the narrower the optical band gap. Photoexcited carriers are believed to be confined inside this sp^2 cluster, and this may explain the high PL efficiency observed in *a*-C:(H) films.[44,45]

IV. SUMMARY AND CONCLUSIONS

The effect of hydrogen dilution during processing on the optical properties of wide band gap amorphous semiconductor *a*-Si:C:H was investigated. The samples were prepared by glow discharge decomposition of tetramethylsilane and were characterized by a variety of optical techniques: spectroscopic ellipsometry, Raman scattering, infrared absorption, UV–VIS–NIR spectrophotometry, and UV photoluminescence. The deposition rate decreased upon hydrogen dilution, while the Si/C ratio remained constant with hydrogen addition. The optical band gap increased as the hydrogen flow rate increased, which is evidenced by spectroscopic ellipsometry and optical absorption measurements. Electron energy loss spectra suggest diminishing contributions from π electrons upon hydrogen dilution. The IR absorption studies show that the concentration of hydrogen which is bonded to carbon decreases systematically upon hydrogen dilution. Hydrogen dilution appears to reduce the size and concentration of the sp^2 bonded carbon cluster, which can be caused by the atomic hydrogen etching of sp^2 clusters. These results are also strongly supported by the shift of the Raman *G* peak position to lower wave numbers. From Raman analysis, it was suggested that H dilution promotes an increase in the bond-angle disorder. Room temperature UV photoluminescence exhibit no correlation with shift in optical band gap.

ACKNOWLEDGMENTS

The authors would like to thank Dr. D. Gracin at Ruder Boskovic Institute, Croatia, for invaluable comments on this article. The authors also appreciate Dr. Sangduk Yoo for critical comments on spectroscopic ellipsometry data. The authors are also grateful to S. Dillon and B. Robin for profilometry and Auger electron spectroscopy, respectively.

[1] Y. Tawada, K. Tsuge, M. Kondo, H. Okamoto, and Y. Hamakawa, J. Appl. Phys. **53**, 5273 (1982).
[2] Y. Hamakawa, D. Kruangam, T. Toyama, M. Yoshimi, S. Paasche, and H. Okamoto, Optoelectron., Devices Technol. **4**, 281 (1989).
[3] P. G. LeComber, J. Non-Cryst. Solids **115**, 1 (1989).
[4] H. Munekata, S. Murasato, and H. Kukimoto, Appl. Phys. Lett. **37**, 536 (1980).
[5] L. R. Tessler and I. Solomon, Phys. Rev. B **52**, 10962 (1995).
[6] Y. Hamakawa, D. Kruangam, T. Toyama, M. Yoshimi, S. Paasche, and H. Okamoto, Opto-Electron. **4**, 281 (1989).
[7] D. Rüter, S. Rolf, and W. Bauhofer, Appl. Phys. Lett. **67**, 149 (1995).
[8] J. Robertson and E. P. O'Reilly, Phys. Rev. B **35**, 2946 (1987).
[9] J. Robertson, Diamond Relat. Mater. **4**, 297 (1995).
[10] F. Alvarez, M. Sebastiani, F. Pozzilli, P. Fiorini, and F. Evangelisti, J. Appl. Phys. **71**, 267 (1992).
[11] S. F. Yoon and J. Ahn, J. Vac. Sci. Technol. A **15**, 1832 (1997).
[12] D. E. Aspnes and A. A. Studna, Appl. Opt. **14**, 220 (1975).
[13] R. K. Sampson and H. Z. Massoud, J. Electrochem. Soc. **140**, 2678 (1993).
[14] J. Fink, Th. Müller-Heinzerling, J. Pflüger, B. Scherer, B. Dischler, P. Koidl, A. Buberzer, and R. E. Sah, Phys. Rev. B **30**, 4713 (1984).
[15] S. Bhattacharyya, C. Vallée, C. Cardinaud, O. Chauvet, and G. Turban, J. Appl. Phys. **85**, 2162 (1999).
[16] X. Zhang, W. H. Weber, W. C. Vassell, T. J. Potter, and M. A. Tamor, J. Appl. Phys. **83**, 2820 (1998).
[17] R. Hillel, M. Maline, F. Gourbilleau, G. Nouet, R. Carles, and A. Mlayah, Mater. Sci. Eng., A **168**, 183 (1993).
[18] M. Cardona and G. Guntherodt, *Light Scattering in Solids III* (Springer, Berlin, 1975), p. 3.
[19] R. J. Nemanich and S. A. Solin, Phys. Rev. B **20**, 392 (1979).
[20] F. Tuinstra and J. L. Koenig, J. Chem. Phys. **53**, 1126 (1970).
[21] A. Richter, H.-J. Scheibe, W. Pompe, K.-W. Brzezinka, and I. Mühling, J. Non-Cryst. Solids **88**, 131 (1986).
[22] S. Prawer, K. W. Nugent, Y. Lifshitz, G. D. Lempert, E. Grossman, J. Kulik, I. Avigal, and R. Kalish, Diamond Relat. Mater. **5**, 433 (1996).
[23] F. Tuinstra and J. L. Koenig, J. Chem. Phys. **53**, 1126 (1970).
[24] S. Bhargava, H. D. Bist, A. V. Narlikar, S. B. Samanta, J. Narayan, and H. B. Tripathi, J. Appl. Phys. **79**, 1917 (1996).
[25] S. Prawer, K. W. Nugent, Y. Lifshitz, G. D. Lempert, E. Grossman, J. Kulik, I. Avigal, and R. Kalish, Diamond Relat. Mater. **5**, 433 (1996).
[26] D. G. McCulloch, S. Prawer, and A. Hoffman, Phys. Rev. B **50**, 5905 (1994).
[27] J. Robertson, Surf. Coat. Technol. **50**, 185 (1992).
[28] J. Wagner, M. Ramsteiner, Ch. Wild, and P. Koidl, Phys. Rev. B **40**, 1817 (1989).
[29] F. Demichelis, F. Giorgis, C. F. Pirri, and E. Tresso, Philos. Mag. B **71**, 1015 (1995).
[30] Y. Katayama, K. Usami, and T. Shimada, Philos. Mag. B **43**, 283 (1981).
[31] H. Wieder, M. Cardona, and C. R. Guarnieri, Phys. Status Solidi B **92**, 999 (1979).
[32] M. H. Brodsky, M. Cardona, and J. J. Cuomo, Phys. Rev. B **16**, 3556 (1977).
[33] G. Lucovsky, Solid State Commun. **29**, 571 (1979).
[34] S. Liu, S. Gangopadhyay, G. Sreenivas, S. S. Ang, and H. A. Naseem, Phys. Rev. B **55**, 13020 (1997).
[35] A. Grill, V. Patel, and B. S. Meyerson, J. Mater. Res. **5**, 2531 (1990).
[36] K. Mui, D. K. Basa, F. W. Smith, and R. Corderman, Phys. Rev. B **35**, 8089 (1987).
[37] H. Shanks, C. J. Faug, L. Ley, M. Cardona, F. J. Demond, and S. Kalbitzer, Phys. Status Solidi B **100**, 43 (1980).
[38] P. Reinke, W. Jacob, and W. Moeller, J. Appl. Phys. **74**, 1354 (1993).
[39] N. F. Mott and E. A. Davis, *Electronic Processes in Non-Crystalline Materials*, 2nd ed. (Clarendon, Oxford, 1979), p. 289.
[40] J. Tauc, R. Grigorovici, and A. Vancu, Phys. Status Solidi **15**, 627 (1966).
[41] F. Demichelis, S. Schreiter, and A. Tagliaferro, Phys. Rev. B **51**, 2143 (1995).
[42] I. Watanabe and M. Inoue, Jpn. J. Appl. Phys., Part 2 **22**, L174 (1983).
[43] R. C. Fang, J. Lumin. **48&49**, 631 (1991).
[44] J. Robertson, Philos. Mag. B **66**, 199 (1992).
[45] Rusli, G. A. J. Amaratunga, and S. R. P. Silva, Thin Solid Films **270**, 160 (1995).